Magnetic Field Effect on Voltage Holding in the MITICA Electrostatic Accelerator

Nicola Pilan, Giuseppe Chitarin, Antonio De Lorenzi, and Gianluigi Serianni

***Abstract*— MITICA is the complete full-scale prototype of a 17 MW heating neutral beam injector for ITER. This experimental device, presently under construction in Padova, includes a negative ion source (H- or D-), and an electrostatic accelerator (1 MV, 40 A, 3600 s). Voltage holding is recognized to be one of the most critical issues for the 1 MV accelerator operations, not only owing to the complex multistage electrostatic accelerator structure, but also for the presence of magnetic field, which is necessary for deflecting the coextracted and secondary electrons as early as possible, before they are accelerated. The required magnetic field is produced by a combination of several sources, such as permanent magnets and current-carrying conductors. To avoid gas breakdown between electrodes, the design of the accelerator shall guarantee that the electrostatic field configuration and the pressure distribution correspond to operating points located far enough on the left side of the well-known Paschen breakdown curve. For this reason, MITICA has been designed so that the (H_2 or D_2) gas pressure multiplied by the distance between electrode ($p \cdot d$) shall not exceed 0.1–0.3 Pa · m. However, indications have been found in literature that the presence of magnetic field might shift part of the left branch of the Paschen curve more to the left, thus reducing the above-defined limit and possibly affecting the voltage holding criteria to be used in MITICA design. To support the design of MITICA at low gas pressure and in the presence of magnetic field, an experimental campaign has been carried out at the high-voltage padova test facility; during this campaign, a field distribution similar to that expected in MITICA has been realized. The magnetic field has been produced using permanent magnets located inside the electrodes or outside the vacuum tank. This paper describes the test assembly, procedure adopted, and the experimental findings; the results have been also successfully compared with simulations of the breakdown process. In certain magnetic field configurations, a clear effect has been recognized, indicating a nonnegligible shift to the left of the lower part of the Paschen Curve.**

***Index Terms*— Fusion reactors, magnetic fields, particle beam injection gas discharges, voltage holding.**

I. Introduction

THE MITICA negative ion neutral beam injector (NNBI) [2], [3] is composed of four main components, namely: a radio frequency (RF) ion source, delivering a negative ion current up to 56 A, a multistage 1 MV electrostatic accelerator, a gas cell neutralizer, and finally an electrostatic residual ion dump.

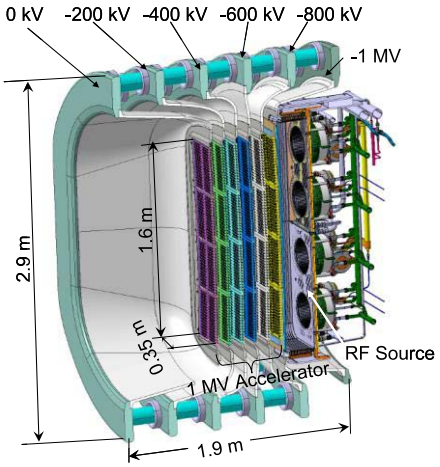

Fig. 1. Section view of the half MITICA beam source electrostatic accelerator, the cut cross section plane is the vertical symmetry plane.

Although the experience in designing and operating the NNBI is based on decades of research and development activities involving many laboratories around the world [4]–[6], [9] the design of MITICA poses several technological challenges because of the unexplored combination of voltage (1 MV), current (56 A), and duration (3600 s) requirements.

This works deals with the voltage holding capability of the electrostatic accelerator, which is based on the multiaperture-multigrid concept [9]. This accelerator has five accelerating grids, polarized at potentials ranging from −1 MV to ground (0 V) with steps of 200 kV.

The negative ion beam is extracted from the beam source by the electric field generated between two dedicated grids: the plasma grid (PG) and the extraction grid (EG), the first one faces the RF plasma generated in the beam source, the second one is located 6-mm downstream of the PG at potential of +10 kV respect to that grid. A set of permanent magnets are embedded in the EG to deflect the electrons which are unavoidably extracted with the negative ions.

Fig. 1 shows a part of the injector with the details of the accelerator. The negative ion beam, extracted from the RF ion source, is composed by 1280 individual beamlets which are guided and focused by an intense electric field through the apertures of the accelerating grids. The high-voltage electrical insulation between the grids relies on vacuum gaps and ceramic spacers. Five sets of alumina spacers (post insulators) are located between the accelerator grids and are therefore subjected to 200 kV dc voltage and to the structural loads

Manuscript received June 28, 2013; revised January 17, 2014 and February 13, 2014; accepted February 20, 2014. Date of publication March 4, 2014; date of current version April 8, 2014. This work was supported by F4E.

The authors are with Consorzio RFX - Associazione EURATOM-ENEA per la Fusione, Padova 35127, Italy (e-mail: nicola.pilan@igi.cnr.it; giuseppe.chitarin@igi.cnr.it; antonio.delorenzi@igi.cnr.it; gianluigi.serianni@igi.cnr.it).

Color versions of one or more of the figures in this paper are available online at http://ieeexplore.ieee.org.

Digital Object Identifier 10.1109/TPS.2014.2307923

(the beam source and the multistage accelerator constitute a cantilever structure sustained by the grounded stage).

The electric field which accelerates the negative ions, unavoidably causes the acceleration of:

1) free electrons existing in the ion source in the vicinity of the PG apertures;
2) electrons produced by stripping reactions in the accelerator as consequence of collisions between the accelerated ions and the background gas;
3) secondary electrons produced by particles impinging on the grids.

Therefore, a transverse magnetic field is necessary in the ion source for assuring a sufficient extraction of the negative ions, while in the accelerator [11] for deflecting all the electrons as soon as possible so that their kinetic energy is limited and they can be directly dumped on the accelerating grids [12].

Given the huge accelerator power (∼56 MW for 1 h beam operating pulse) the magnetic filter is fundamental to avoid both grid damages and excessive power dissipations.

The magnetic field inside the beam source consists of two components:

1) a local magnetic field produced by permanent magnets embedded in the extraction grid (EG) and in the subsequent accelerating grids (AGs);
2) a long range component, produced by a current flowing in the first grid, called PG and in shaped conductors. This field exists both in the Ion source and in the accelerator.

Because of the magnetic field produced inside the electrostatic accelerator, the stripped electrons can be deflected and eliminated from the negative ion beam. To provide the possibility of independent control of the long range field in the beam source and in the accelerator, a couple of external trimming magnetic field coils (TMFC) have been also proposed. The TMFC would be located outside the vacuum vessel and produce a horizontal magnetic field perpendicular to the beam direction. Details of the magnetic configuration and the location of magnetic field sources are available in [10] and [12].

Fig. 2 shows the electric field distribution in a horizontal plane across the accelerator center.

As shown in Fig. 2, the equipotential surfaces completely surround the negative ion source passing between the accelerating grids. At nominal voltage, the electrostatic field strength is ∼2–3 kV/mm inside the electrostatic accelerator and ∼1 kV/mm in the region between the ion source and the vessel.

The (H_2 or D_2) gas pressure is in the range 10^{-5}–10^{-1} Pa depending on the operation type, for example, high-voltage conditioning (without beam) or beam extraction at high current [2]. The details of the pressure maps are available in [13] and [14].

Although many efforts have been dedicated in past to study the voltage holding in high vacuum ($p < 10^{-3}$ Pa), this topic still remains an open issue, especially for the large gap configurations because the physical phenomena is not completely understood [15]; on the other hand, the electrical breakdown in low-pressure gas (10^{-1}–10^{0} Pa) is described by the Townsend gas discharge theory [16] represented by the Paschen ($p \cdot d$) curve. The effect of magnetic field on the Paschen curve is far from being straightforwardly quantified.

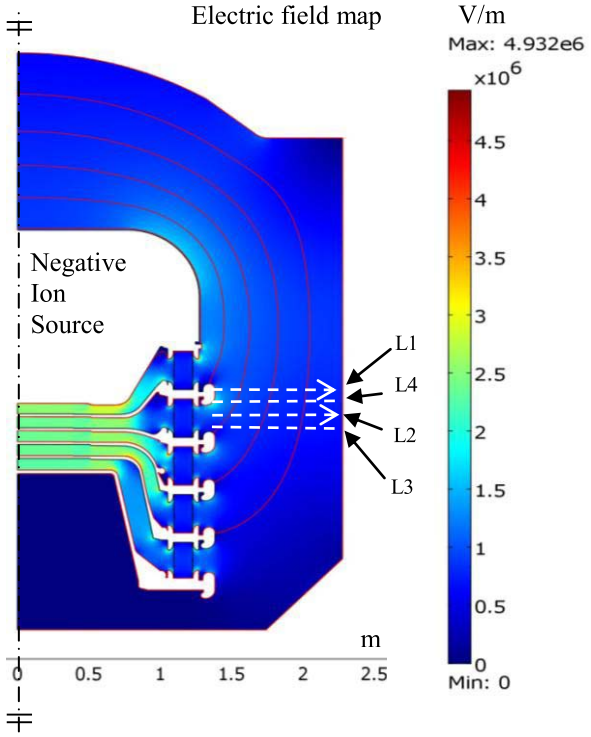

Fig. 2. Horizontal cross section of the MITICA accelerator: electric field map and equipotential lines. The dotted lines L1, L2, L3, and L4 are the paths where the MITICA magnetic fields have been calculated, see Fig. 5.

Several papers [17]–[19] describe the effect of the magnetic field on the gas discharge and demonstrate that a magnetic field perpendicular to the electric field can shift the Paschen curve toward the left [17]. This phenomenon could jeopardize voltage holding during the beam extraction at relatively high pressure, if the Paschen curve approaches the accelerator operating region. In [17], two complementary criteria for evaluating the magnetic field effects on the gas discharge are discussed. Unfortunately, such results are not directly applicable to the MITICA electrostatic accelerator because they refer to the ideal configuration having both E and B uniformly distributed in space. Moreover, such criteria refer to relatively low voltage ($U < 10$ kV) and E/p ratio.

Thus, we tried to verify if the accelerator operating region (in terms of pressure, distance, and voltage) is sufficiently far from the Paschen curve in presence of magnetic field during the beam extraction.

It is important to underline that in the HVPTF experiments and in MITICA, the magnetic field strength is not identical and far from uniform; the same remark applies to the electrostatic field as well. Therefore, a 3-D Monte Carlo model has been adopted to interpret the experimental results of HVPTF and to predict the behavior of MITICA.

II. Experimental Campaigns on the Magnetic Field Effect at the HVPTF

The HVPTF (described in [1]) is equipped with a cylindrical stainless steel vacuum chamber, having 597 mm radius and

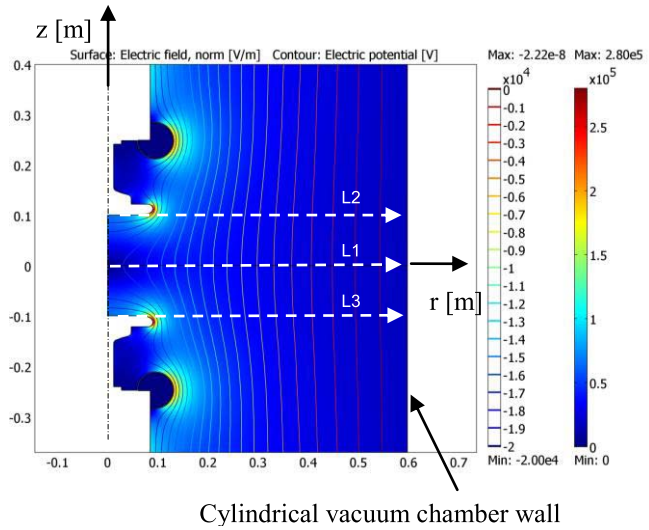

Fig. 3. Electric field map of HVPTF when both electrodes are polarized at the same potential (−20 kV). The dotted lines L1, L2, and L3 are the paths where magnetic fields have been calculated, see Fig. 5. L2 and L3 have the same magnetic field distributions.

2450 mm length. A H_2 gas injection system together with rotative and turbomolecular pumps allow a fairly precise control of the pressure in the range from 10^{-5} and 1 Pa. A pair of electrodes having symmetric layout, can be polarized with respect to the grounded vessel by two independent power supplies.

The HVPTF was originally designed for voltage holding tests in high vacuum between flat or shaped electrodes [20] and its metallic vacuum chamber was chosen to be as large as possible to avoid any effect on voltage holding between electrodes. However, when operating the chamber at higher gas pressure, the system approaches the left branch of the Paschen curve, and we expect that the gas breakdown initiates between one electrode and the vessel, exactly where the largest product of pressure and electrode gap ($p \cdot d$) is achieved. Preliminary experiments without magnetic field confirmed this expectation.

Thus, to avoid that the (major) effect of the electric field between the electrodes and the ground (long gap) could be mixed up with a (minor) effect of the electric field between the electrodes (short gap), it was decided to carry out all experimental tests by polarizing both electrodes at the same potential and considering the gas discharge a process mainly directed radially. In this condition, the two electrodes behave like a single one, and the vacuum chamber acts as the other active electrode. Fig. 3 shows the electric field distribution in HVPTF when both electrodes are polarized at the same potential (−20 kV).

Two experimental campaigns have been carried out for investigating the magnetic field effect on the Paschen curve adopting different permanent magnet setups. For the first campaign, two stainless steel electrodes 180 mm in diameter were provided with a set of embedded Sm–Co permanent magnets having $4.6 \times 5.6 \times 80$ mm size and 1.1 T remanence. Fig. 4 shows the magnet position inside the electrodes, which are located 1.5 mm below the electrode surfaces. The permanent magnets were oriented to have a magnetic field almost parallel

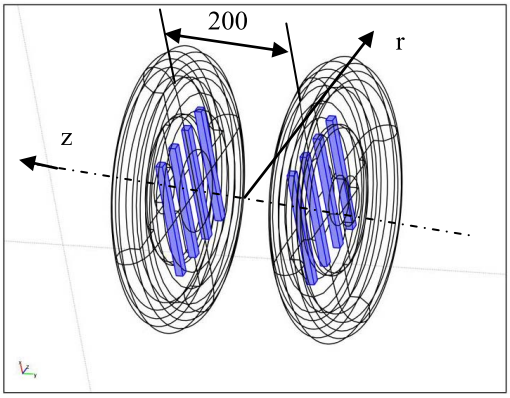

Fig. 4. View of the stainless steel electrodes adopted in the first campaign. Four small permanent magnets are embedded in each electrode (first campaign). The magnets are highlighted in blue. Dimension is in mm.

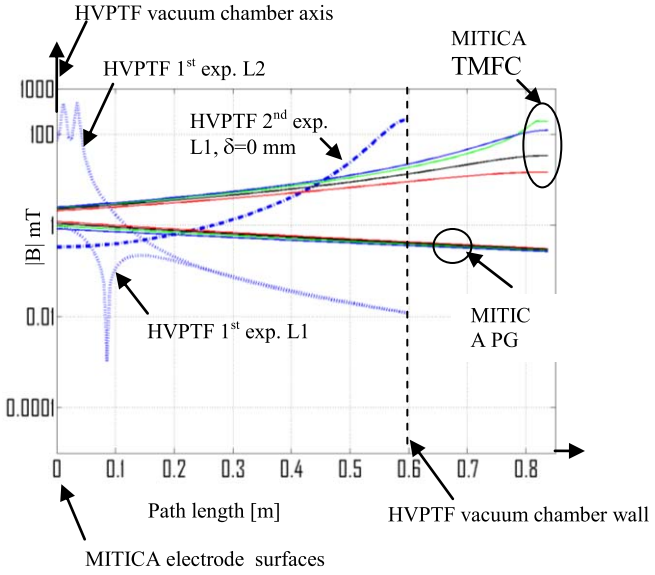

Fig. 5. Distributions of magnetic field strength along path L1 to L4 for MITICA, L1 and L2 for HVPTF, see together with Figs. 2 and 3. The case with $\delta = 25$ mm in the second experimental campaign can be obtained shifting the dot dash curve toward right by 25 mm.

to the electrodes surfaces. Both electrodes were polarized negatively at the same potential, in this way the HVPTF chamber was the anode. This configuration approximately reproduces the field distribution in MITICA where the magnetic field between the electrostatic accelerator and the vessel is almost parallel to the grids.

The second experimental campaign was carried out using a large Nd–Fe–B permanent magnets, having a size of $110.6 \times 89 \times 19.5$ mm and a remanence of 1.2 T. The magnets were located outside the vacuum chamber at a distance δ from the chamber wall. Because both electrodes were polarized positively at the same voltage, the vacuum chamber acted as the cathode.

The aim of the two HVPTF setups was to reproduce approximately the electric and magnetic field configuration expected in MITICA.

Fig. 5 shows the magnitude of the magnetic field produced by the MITICA PG and external coils (TMFC), along the dotted paths (L1, L2, L3, and L4) defined in Fig. 2.

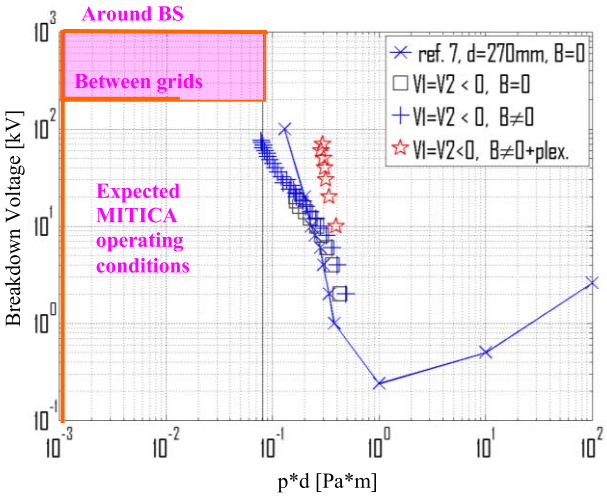

Fig. 6. Results of the first experimental campaign on HVPTF: Paschen-like curve with H_2 gas. Pink color: the MITICA working regions. The high-voltage conditioning procedure is represented by the vertical line from 0 to 1 MeV at very low pressure with $p^*d < 10^{-3}$ Pa · m.

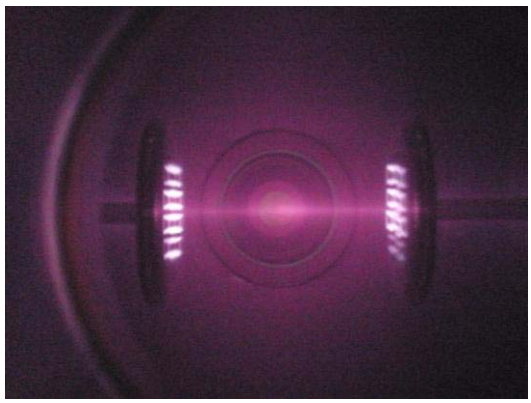

Fig. 7. Glow phenomena, between electrodes during the first experimental campaign, $V1 = V2 = -20$ kV, B $\neq 0$.

A magnetic field of similar strength (100–200 mT) was produced around the electrodes on the HVPTF. In the first campaign, the maximum field was on the inner electrodes, near the vacuum chamber axis, for the second campaign, the maximum was on the vacuum chamber surface. The magnitude of the magnetic field along the dotted paths L1, L2, and L3 of Fig. 3 in HVPTF is reported in Fig. 5 both for the first and for the second experimental campaigns.

The results of the first campaign are summarized in Fig. 6 in term of Paschen-like curve, that is, breakdown voltage as a function of pressure multiplied by gap length ($p \cdot d$ product). All experimental points where collected at constant voltage starting at low pressure and increasing the pressure up to the Townsend breakdown.

As already mentioned, the breakdown always occurred between an electrode and the grounded chamber; therefore, a nominal gap length $d = 0.6$ m was assumed in the $(p \cdot d)$ product. The Paschen-like curve obtained in this way was generally consistent with the standard data reported in literature for a similar gap length and with no magnetic field [7], [8]. The Townsend breakdown between one electrode and the vessel always occurred suddenly and caused a voltage collapse (arc-type discharge).

As shown in Fig. 6, no appreciable effect of the magnetic field on voltage holding was evidenced during the first experimental campaign. The HVPTF experimental data in Fig. 6 without magnetic field are reported by black squares while the data with magnetic field are marked by plus signs. Only a small leftward deviation of the left branch of the Paschen curve with respect to the standard one was observed both with and without magnetic field at higher voltages.

This small deviation has been related to the local ionization (glow phenomena) visible between the two electrodes, when they were both polarized at the same negative potential (-10 kV) inside the grounded chamber. This glow was visible already before the sudden breakdown to ground occurred. Because of this peculiar geometry, positive ions are likely attracted toward the center of the vacuum chamber and they oscillate radially between the electrodes across the vacuum chamber axis; this configuration constitutes a sort of electrostatic ion trap and Fig. 7 shows this glow in presence of magnetic field. The bright spots correspond to the position of the embedded magnets inside the electrodes. The same glow (without the bright spots due to the magnets presence) and the same breakdown voltage to ground and almost same pressure were observed in absence of magnetic field.

Our interpretation is that the discharge toward the grounded metallic chamber is facilitated by the ionizing collisions of the trapped H_2^+ ions with neutrals hydrogen molecules. This interpretation was confirmed when a cylindrical pipe made of Plexiglas was placed around the gap between electrodes, to intercept any positive ion trajectories. The corresponding experimental points are reported in Fig. 6 (red star markers). These points show that the deviation of the Paschen curve caused by the electrostatic trap is no longer present, because the positive ions were prevented to cross radially the gap between the electrodes many times.

In the HVPTF first experimental campaign, the maximum magnetic field (100–200 mT) was close to the value foreseen in MITICA, but its spatial gradient was very high (the magnetic field strength decreased to 1 mT in few centimetres). Thus, these results appeared to be not exhaustive and a second experimental campaign was carried out adopting a configuration having a more uniform distribution of the magnetic field. As it was not possible to install larger magnets or active coils on the electrodes inside the HVPTF chamber, a large permanent magnet was attached outside the vacuum chamber wall. A positive voltage ($V1 = V2 > 0$) was applied to the electrodes, so that the grounded vacuum chamber acted as a cathode. The maximum magnetic field was controlled by changing the distance δ between the magnet and the outer surface of the chamber.

As in the previous campaign, the experimental Paschen-like curve was obtained by applying a voltage while increasing the pressure in the chamber, up to the Townsend discharge initiation.

A considerable deviation of the left branch of the Paschen-like curve has been observed with this configuration, as shown in Fig. 8. Moreover, the arc discharge has been replaced

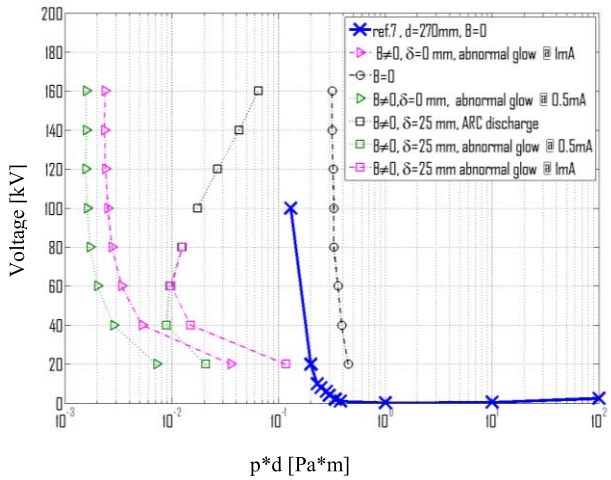

Fig. 8. Paschen-like curves in H_2, second experimental campaign. Triangular markers correspond to the cases with $\delta = 0$ mm, squared markers correspond to the cases with $\delta = 25$ mm. Circular and X markers: cases with $B = 0$ [T]. Black lines: arc discharges. Green lines: cases with abnormal glows at 0.5 mA. Pink lines: cases with abnormal glows at 1 mA. Blue line: reference curve.

by a steady-state glow discharge (abnormal glow) with no sudden voltage collapse. In this case, the discharge pressure was dependent on the current limit of the power supply (0.5 or 1 mA as shown in Fig. 8). Only the cases with small magnetic field ($B = 0$ or $\delta = 25$ mm) at higher voltages were still characterized by the voltage breakdown. However, both arc and glow discharges are consequences of a Townsend discharge and are considered unacceptable in MITICA accelerator.

The most relevant effects were observed in terms of variation of breakdown pressure, in fact, in the case $\delta = 0$ mm (magnet in contact with the vacuum chamber) the current limit (0.5 or 1 mA) was achieved for a pressure about two orders of magnitudes lower than in the corresponding breakdown pressure without magnetic field.

It is also interesting to notice that, when the magnet was 25 mm far from the vacuum vessel wall, the lower part of the Paschen-like curve became belly shaped. In this case, some $(p \cdot d) = \text{const}$ (vertical) lines cross the curve twice. This implies that, for a fixed pressure, the breakdown will occur only within a lower and an upper voltage limit. Thus, we have experimentally found that after a certain pressure, voltage, and magnetic field are applied without breakdown, the breakdown occurs at lower voltage rather than at higher voltage.

These unexpected experimental observations have been explained as follows: any charged particle in a uniform magnetic field $\bar{B}$ and electric field $\bar{E}$ between two electrodes follows a cycloidal trajectory having an amplitude Δ long the electric field direction:

$$\Delta = \frac{m \cdot E}{q \cdot B^2}. \tag{1}$$

If the magnetic field is large enough, Δ becomes smaller than the electrode gap and the charged particles cannot reach the opposite electrode. In this case, the trajectory becomes a composition of many cycloids. This motion corresponds to a

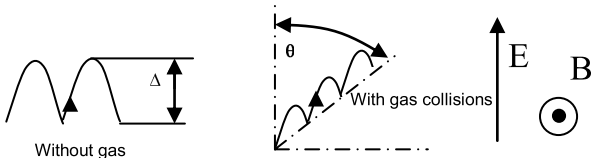

Fig. 9. Examples of electrons trajectories in uniform magnetic and electric field.

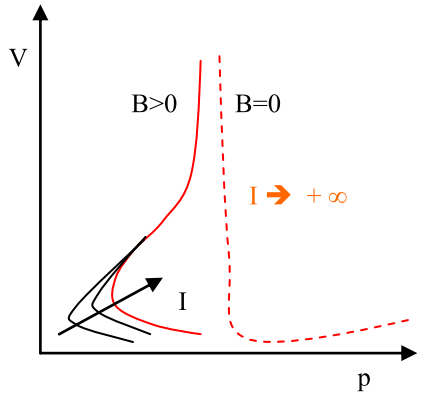

Fig. 10. Qualitative representation of magnetic field effect on breakdown voltage and pressure in a system with current-controlled power supplies.

free drift with an average drift velocity described by

$$\overline{v}_d = \frac{\overline{E} \times \overline{B}}{B^2}. \tag{2}$$

As the drift velocity is perpendicular both to $\overline{E}$ and $\bar{B}$, collisions with other particles become more likely because the cycloids substantially extend the total length of the particle trajectories. If the energy gained by particles between collisions is larger than the ionization potential, further ionization is produced. In these conditions, increasing the magnetic field, ionization, and breakdown becomes easier because the number of collisions increases.

After each collision, the particle trajectory proceeds along a direction inclined by the angle θ with respect to the electric field E, as shown in Fig. 9. Therefore, the avalanche discharge direction results to be oblique with respect to the electric field direction.

This process occurs more efficiently at low gas pressure. At high gas pressure, the energy gained by the particle is no longer sufficient for ionizing the new particles at the next collision.

At higher voltage (i.e., higher E) Δ becomes larger and the Paschen curve deviation is reduced as shown in Fig. 8. Above 70–100 kV (with $\delta = 25$ mm), the left branch of the Paschen curve is little influenced by magnetic field. The general behavior of the curve depending on magnetic field can be summarized by the shape proposed in Fig. 10.

Fig. 10 shows a qualitative representation of the magnetic field effect on breakdown voltage and pressure in a system with current-controlled power supplies. Solid lines correspond to the initiation of a glow discharge with different power supply currents (1–10 mA) in a given magnetic field configuration, at very low pressure. The dotted line corresponds to zero magnetic field. The red color indicates the onset of an arc discharge, in which the power supplies cannot limit the current.

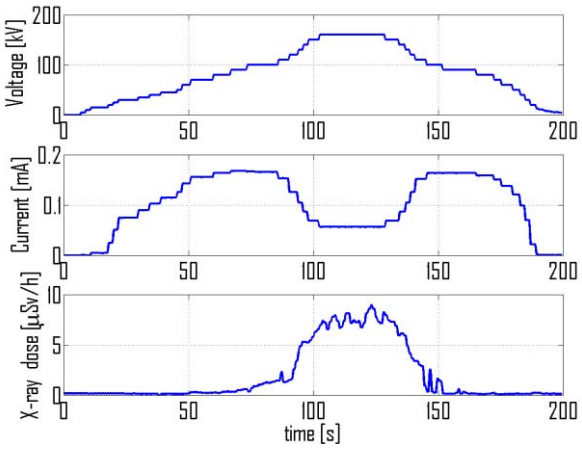

Fig. 11. Test at constant pressure $p = 1.36\ 10^{-3}$ Pa with magnetic field (second experimental campaign). One electrode is energized positively (the other is connected to ground). The X-ray equivalent radiation dose rate was measured 1 m outside of the vacuum chamber.

The shape shown in Fig. 10 has been confirmed by further investigations using a different experimental procedure. The same shape was obtained by keeping a constant pressure and by increasing the voltage up to the glow discharge occurrence. Fig. 11 shows the experimental results as a functions of time during a test carried out at $1.36\ 10^{-3}$ Pa H_2 pressure, when the above-described large magnet was in contact with the outer surface of the vessel ($\delta = 0$ mm).

It is worth noticing that discharge current reaches the maximum value of 0.168 mA when the voltage is 90 kV. Further increase of the voltage, decreases the current to a factor of $\sim$2. Although this singular aspect can be inferred from [15, Fig. 17], it is not directly described in the literature, to our knowledge. Fig. 11 also shows the X-ray emission measured in term of equivalent dose rate outside the vacuum chamber. Although this measurement is qualitative, it shows that when the voltage is higher than 90–100 kV, the current decreases, but the X-ray dose rate increases considerably.

III. Monte Carlo Numerical Simulation of the Townsend Discharge With Magnetic Field

A Monte Carlo code has been developed to explain the experimental results and to predict the breakdown pressure on the left branch of the Paschen curve for a generic device in presence of magnetic and electric fields.

There are some possible numerical schemes to face the problem [21] but two important constrains have to be considered: 1) magnetic and electric fields in MITICA and in HVPTF are not uniform in space and 2) the domain to be simulated is characterized by shaped geometries. In view of this geometrical complexity, the numerical code has been developed looking for a simple solution capable only of distinguishing if an assigned configuration produces (or not) an exponential growth of electrons.

A. Code Description

The code is based on a ray-tracing algorithm, which numerically integrates the equation of the motion for a swarm of electrons. A matrix M of dimension $(7 \cdot n)$ is used for representing position, velocity, and flight time of a population of n electrons. The matrix is updated step by step during the integration of the motion. When an electron touches the wall and disappears, the corresponding column of M is deleted, on the other hand when an electron appears a new column of M is considered.

The code includes the essential aspects of the classical Townsend discharge model and reproduces the exponential multiplication of the electrons, that is, the breakdown occurrence. The ionization of the neutral gas molecules, which depends on positive ions collisions against neutral gas, is not considered.

The classic (3) for plane parallel electrodes (without magnetic field) describes the current drained between electrodes owing to the neutral gas ionization

$$i = \frac{i_0 \cdot \exp(\alpha \cdot L)}{1 - \xi \cdot [\exp(\alpha \cdot L) - 1]} \tag{3}$$

where α and ξ are, respectively, the first and the second Townsend ionization coefficients.

The first coefficient α has been computed using the classic formula as follows:

$$\frac{\alpha}{p} = A_1 \cdot \exp\left(-\frac{A_2}{E/p}\right) \tag{4}$$

where the symbol E is the electric field strength, p is the background gas pressure, and A_1 and A_2 are two constant coefficients depending on gas type. For Hydrogen $A_1 = 3.82\ [\mathrm{Pa}^{-1} \cdot \mathrm{m}^{-1}]$ and $A_2 = 93.6\ [\mathrm{V} \cdot \mathrm{Pa}^{-1} \cdot \mathrm{m}^{-1}]$ have been used, according to [22].

Because (4) summarizes both ion and electron contributions to ionization, it has been implemented in place of the ionization cross section of the background gas. This choice has allowed simplifying the simulations even if possible avalanches of positive ions due to the background gas ionization cannot be simulated.

The second ionization coefficient ξ is the yield coefficient because of H_2^+ ion impact on the metallic electrode surfaces, and was derived from [23].

The background gas ionization is described statistically according to the Monte Carlo algorithm [30]. During each integration step, new ionization events are randomly introduced, thus to obtain a relative increment (RI) of the number of electrons in agreement with the formula

$$d(\mathrm{RI}) = \exp(\alpha \cdot dl) - 1. \tag{5}$$

The computation of the electrons trajectories is carried out by solving the relativistic equation of the motion by using the fourth-order adaptive RK5(4) 7M Runge–Kutta algorithm described in [24]. The time step is limited in order to have $\alpha \cdot dl \ll 1$.

Because we are only interested in understanding whether the gas discharge occurs (or not) for an assigned configuration, we do not need to model the full discharge evolution. Thus magnetic and electric fields are calculated by external programs, in a manner which is not fully self-consistent with the motion of the charged particles.

The motion of electrons is relativistic because the maximum acceleration voltage in MITICA is 1 MV so the relativistic equations of motion, reported in (6)–(8), have been considered

$$\bar{u} = \gamma \cdot \frac{\bar{v}}{c} \tag{6}$$

$$\gamma = \sqrt{1 + \bar{u}^t \cdot \bar{u}} \tag{7}$$

$$\frac{d}{dt}(m \cdot c \cdot \bar{u}) = q \cdot \{\bar{E} + \bar{v} \times \bar{B}\} - m \cdot \sigma_{\text{tot}} \cdot N \cdot v \cdot \bar{v}. \tag{8}$$

In previous equations, $\bar{v}$ is the particle velocity in the laboratory system of coordinates, m and q are the particle mass and charge, respectively, and γ is the relativistic factor ($\gamma = 1/\sqrt{1 - v^2/c^2}$). The total cross section σ_{tot} for interactions of electrons with neutral hydrogen has been obtained from [25, Fig. 2].

The positive ion trajectories have been calculated considering only the electric field, because the magnetic field effect is almost negligible on them.

Moreover, we have assumed that the motion of the ions starts with zero velocity and is not relativistic. Hence, it is possible to demonstrate [26] that the ion trajectories in an electric (conservative) field does depend neither on their charge and mass, nor on applied voltage.

On this basis, a map of the (collisionless) motion for the ions has been determined in such a way that each point in the domain can be related to an impact position on one of the electrodes. This map is calculated only once, thus avoiding recalculating the impact position every time an ion is produced inside the volume. Further collisions of the ions before hitting the electrodes are neglected. However, each collision of ions on the electrodes generates one or more secondary electrons according to the parameter ξ and the ion impact energy.

The electric field has been calculated using a FEM model (Comsol Multiphysics 3.5 [27]). The stationary magnetic field generated by the coils have been calculated integrating analytically the first elementary Laplace's equation for filamentary conductors. The magnetic field produced by the permanent magnets has been calculated basing on the analytical expression given in [31].

Several primary electrons, typically 60 000/m^3, are randomly generated and uniformly distributed in the simulation domain; their initial velocities are assigned according to background gas temperature.

The breakdown is recognized when the number of electrons tends to diverge during the simulation.

B. Code Validation

The code was validated against the experimental results described in Section II. The benchmark was carried out up to 160 kV which is the maximum voltage achieved in the experiments. The code was applied to the simulation of the first and the second experimental campaigns. In the first case, the simulations did not highlight any magnetic field effects. This is consistent with the experimental results, as shown in Fig. 12.

The experimental data of Fig. 12 are the ones shown in Fig. 6.

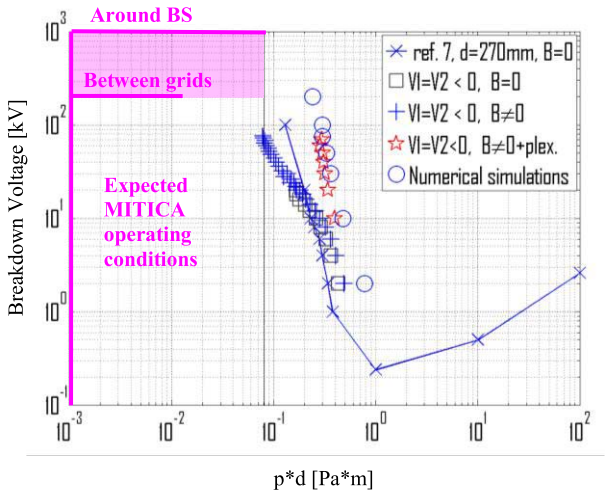

Fig. 12. First experimental campaign: comparison of numerical simulations and experimental results, H_2 Paschen curve ($d = 0.6$ m in HVPTF corresponds to the radius of the vacuum chamber).

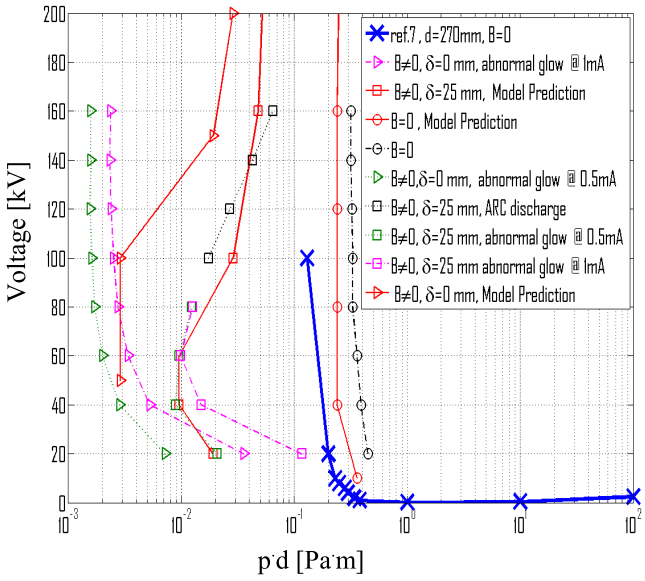

Fig. 13. Second campaign: comparison of numerical simulation and experimental results, H_2 Paschen curve, ($d = 0.6$ m in HVPTF corresponds to the radius of the vacuum chamber). The experimental data are the same of Fig. 8 and the numerical results are indicated by red lines.

The experimental points of Fig. 12 show a $p \cdot d$ product in the range 0.1–1 Pa $\cdot$ m, which is in agreement with the results of the numerical simulations. It is interesting to note that the numerical simulation results (blue circles) fit very well the experiments with the Plexiglas pipe (red stars). Probably this is because the ionization effect of the positive ions on H_2 is neglected in the simulation. As already mentioned in Section I, the small leftward deviation of the experimental data at higher energies (blue crosses and black squares) is most likely because of the ionization of the neutral molecules caused collision with positive ions.

Fig. 13 compares the same diagram experimental results and simulations concerning the second experimental campaign, so the experimental data of Fig. 13 are the ones shown in Fig. 8.

Fig. 13 shows that the numerical simulation results somehow predict the belly-shaped modification of the left branch of

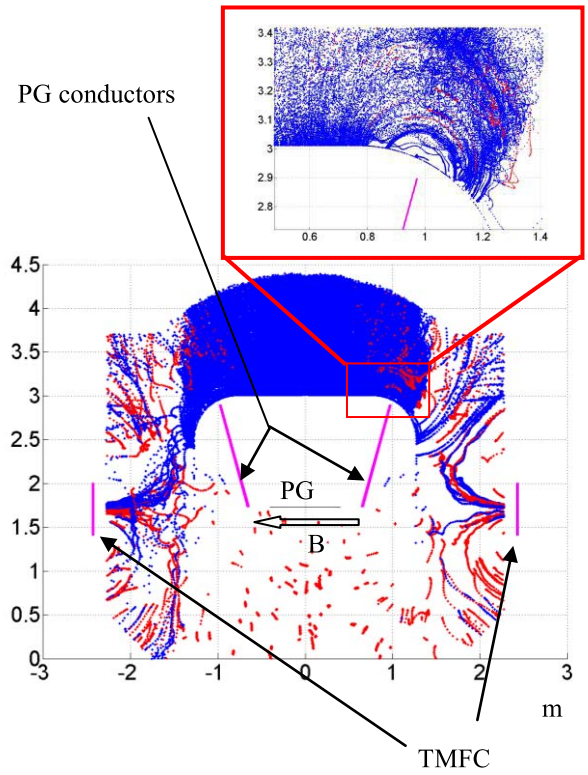

Fig. 14. Top view of MITICA showing electron avalanches and breakdown caused by high pressure ($p = 0.2$ Pa). Red lines: primary electrons. Blue lines: secondary electrons). Total voltage between beam source and grounded vessel is $U = 200$ kV.

the Paschen curve due to the magnetic field. Both the case with $\delta = 25$ mm and with no magnetic field are in good agreement with the simulations. For $\delta = 0$ mm (large magnetic field on the cathode surface), a less satisfactory agreement has been found at higher voltages.

IV. Evaluation of Magnetic Fields Effect on the MITICA Electrostatic Accelerator

Even if the benchmark was not fully satisfying at high voltages with strong magnetic fields, the Monte Carlo code has been applied to the MITICA accelerator, which is designed to operate with a negative ion beam in H_2 gas pressure up to 5×10^{-2} Pa with a voltage up to 1000 kV.

For the simulations, the 2-D electric field map shown in Fig. 2 was used (scaled according to the accelerator voltage) together with a 3-D magnetic field map calculated by integrating the elementary Laplace's equation.

Fig. 14 shows a typical distribution of electrons in the simulated MITICA accelerator during a breakdown. The red lines indicate the trajectories of the primary electrons, and the blue lines indicate those of the secondary electrons. The pink lines represent the position of the magnetic field sources, both the PG (and related busbars) and the TMFC coils as indicated in the figure. The picture shows that both species tend to be trapped by the magnetic field lines.

As an example, a maximum voltage of 200 kV between beam source and vessel was considered (the potential of intermediate electrodes was scaled proportionally) with a pressure of 0.2 Pa around the beam source (normal value

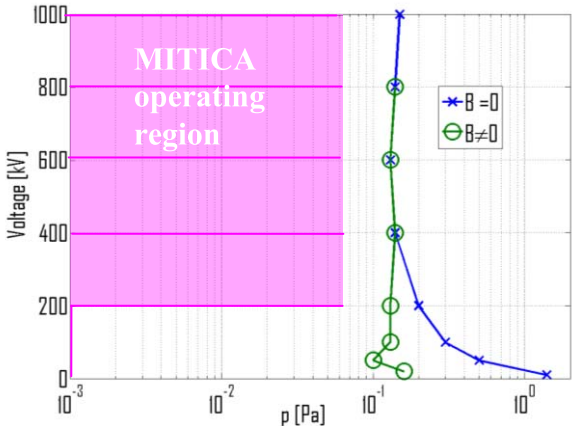

Fig. 15. Effect of magnetic field on gas discharge for the MITICA electrostatic accelerator. Numerical model predictions.

is 0.05 Pa). The simulation shows that a discharge can occur in the rear part of the source, where the gap length is larger and the peak of secondary electron density is expected. This example allows to understand the behavior of the system in case of excessive gas pressure.

Fig. 15 shows the Monte Carlo code predictions for MITICA operation in H_2 and compares the cases with and without magnetic field. In this figure, the breakdown voltage calculated by simulations is reported as function of the sole H_2 pressure p to avoid the ambiguity caused by the definition of the gap length.

Although these simulations do not consider a full 3-D electric field map and the largest electrode gap considered is only 1.2 m (instead of 2.5 m) because of the 2-D planar geometry assumed, the prediction shown in Fig. 15 seems credible.

The numerical simulations show that, in spite of the deviation of the left branch of the Paschen-like breakdown curve, caused by the long range magnetic field, the curve does not overlap the expected operating conditions. In any case, the use of TMFC coils in MITICA gives the possibility to implement an high-voltage conditioning procedure avoiding the belly shape of the left branch of the Paschen curve: starting at the lowest pressure ($p < 10^{-4}$ Pa), the voltage could be raised to the maximum value compatible with very low pressure, without magnetic field (conditioning at low pressure). Then the pressure could be increased up to nominal value (3–5×10^{-2} Pa). From this point, the voltage is raised again up to the desired value, exploiting the improvement of voltage holding due to higher pressure effect [15]. Finally the magnetic field can be applied without intercepting the deviated Paschen breakdown curve.

V. Conclusion

The effect of magnetic field on voltage holding across a gap in low-pressure gas has been studied both by experiments and numerical simulations. A deviation to the left of the left branch of the H_2 Paschen curve owing to magnetic field has been observed.

The classic numerical description of the Townsend breakdown mechanism in low-pressure gas has been adapted, taking

into account the magnetic field and using a Monte Carlo approach for the gas ionizing collisions. This numerical approach appears suitable to predict the breakdown gas pressure on the left branch of the Paschen curve.

This tool has been used to simulate and predict the behavior of MITICA. The numerical results, shown in Fig. 15, do predict some effects of the magnetic field on the Townsend breakdown. These effects appear to be particularly evident at lower voltage, as the magnetic field tends to extend the electron trajectories, with respect to the ionization mean free path, only in presence of a low electric field.

The model predictions, in Fig. 15, show that breakdown could occur at about 0.1 Pa in presence of magnetic field. This pressure is greater than the expected operating pressure around the MITICA electrostatic accelerator, which is $\sim$0.05 Pa.

This gives a pressure safety margin of about 2 with respect to Townsend breakdown, and this number is not very much affected by the presence of the magnetic field.

Although this margin could be considered quite small in absolute terms, it appears difficult to increase it by design, as it is intrinsically based on the accelerator topology and size. The extraction of high beam current requires operating up to a pressure up to 0.3 Pa inside the source. The pressure around the source can therefore change from 10^{-6} up to 0.05 Pa.

In general, the gas discharge occurrence could be avoided by reducing the $p \cdot d$ product and therefore the gap length. However, the operation at very low pressure would be obviously hindered if the gap length is reduced, as voltage holding in high vacuum ($p < 10^{-5}$ Pa) typically scales with the square root of the gap length.

In absence of other design choices, we do accept this limited safety margin, having no other evidence which can compromise the accelerator nominal working parameters.

In addition, there is some uncertainty on the magnetic field effect in high vacuum ($p < 10^{-5}$ Pa). The study reported in [8] shows that there is almost no magnetic field effect at very low pressure, but it is not clear whether a very strong magnetic field could affect the voltage holding at pressure slightly higher.

REFERENCES

[1] A. De Lorenzi, N. Pilan, L. Lotto, M. Fincato, G. Pesavento, and R. Gobbo, "HVPTF—The high voltage laboratory for the ITER neutral beam test facility," *Fusion Eng. Des.*, vol. 86, nos. 6–8, pp. 742–745, 2011.

[2] R. Hemsworth *et al.*, "Status of the ITER heating neutral beam system," *Nucl. Fusion*, vol. 49, no. 4, p. 045006, 2009.

[3] P. Zaccaria *et al.*, "Progress in the MITICA beam source design," *Rev. Sci. Instrum.*, vol. 83, no. 2, p. 02B108, 2012.

[4] Y. Takeiri *et al.*, "High-power and long-pulse injection with negative-ion-based neutral beam injectors in the large helical device," *Nucl. Fusion*, vol. 46, no. 6, pp. S199–S210, 2006.

[5] E. Speth *et al.*, "Overview of the RF source development programme at IPP Garching," *Nucl. Fusion*, vol. 46, no. 6, pp. S220–S238, 2006.

[6] T. Inoue *et al.*, "1MeV, ampere class accelerator R&D for ITER," *Nucl. Fusion*, vol. 46, no. 6, pp. S379–S385, 2006.

[7] T. Inoue *et al.*, "Development of a large volume negative-ion source for ITER neutral beam injector," *Rev. Sci. Instrum.*, vol. 71, no. 2, pp. 744–746, 2000.

[8] K. Watanabe *et al.*, "DC voltage holding experiments of vacuum gap for high energy ion sources," *J. Appl. Phys.*, vol. 72, no. 9, pp. 3949–3956, Nov. 1992.

[9] R. S. Hemsworth, "Some lessons from long pulse operation of negative ion sources and accelerators," *Nucl. Fusion*, vol. 46, no. 6, pp. S236–S249, 2006.

[10] G. Chitarin, N. Marconato, P. Agostinetti, G. Serianni, and P. Sonato, "Flexible magnetic design of the MITICA plasma source and accelerator," in *Proc. AIP 3rd Int. Symp. NIBS*, vol. 1515. 2013, p. 217.

[11] B. Heinemann *et al.*, "Design of the 'half size' ITER neutral beam source for the test facility ELISE," *Fusion Eng. Des.*, vol. 84, nos. 2–6, pp. 915–922, 2009.

[12] G. Chitarin *et al.*, "Optimization of the electrostatic and magnetic field configuration in the MITICA accelerator," *Fusion Eng. Des.*, vol. 88, nos. 6–8, pp. 507–511, 2013.

[13] E. Sartori and P. Veltri, "AVOCADO: A numerical code to calculate gas pressure distribution," *Vacuum*, vol. 90, pp. 80–88, 2013.

[14] E. Sartori, S. Dal Bello, G. Serianni, and P. Sonato, "Distribution of the background gas in the MITICA accelerator," in *Proc. 3rd Int. Symp. NIBS Conf.*, 2013, pp. 121–128.

[15] F. Rohrbach, "Isolation sous vide," CERN, Meyrin, Switzerland, Tech. Rep. 71-5, 1971

[16] J. M. Meek and J. D. Craggs, *Electrical Breakdown of Gases*. London, U.K.: Oxford Univ. Press, 1953.

[17] A. E. D. Heylen, "Electrical ionisation and breakdown of gases in a crossed magnetic field," *IEE Proc. A Phys. Sci., Meas. Instrum., Manag. Educ., Rev.*, vol. 127, no. 4, pp. 221–244, May 1980.

[18] S.-Z. Li, "Influence of magnetic field on the electrical breakdown characteristics in cylindrical diode," *Phys. Plasmas*, vol. 11, no. 7, pp. 3443–3448, 2004.

[19] G. R. Giovinda Raju and G. R. Gurumurthy, "Electrical breakdown of gases between coaxial cylindrical electrodes in crossed electric and magnetic fields," *IEEE Trans. Electr. Insul.*, vol. 12, no. 5, pp. 325–334, Oct. 1977.

[20] A. De Lorenzi, N. Pilan, and E. Spada, "Progress in the validation of the voltage holding prediction model at the high-voltage Padova test facility," *IEEE Trans. Plasma Sci.*, vol. 41, no. 8, pp. 2128–2134, Aug. 2003.

[21] G. G. Lister, "Low-pressure gas discharge modelling," *J. Phys. D, Appl. Phys.*, vol. 25, no. 12, pp. 1649–1680, 1992.

[22] A. Zastawny, "Standardization of gas amplification description in proportional counters," *Nucl. Instrum. Methods Phys. Res. A, Accel., Spectrom., Detectors Assoc. Equip.*, vol. 385, pp. 239–242, Jan. 1997.

[23] G. Fubiani, H. P. L. de Esch, and A. Simonin, "Modeling of secondary emission processes in the negative ion based electrostatic accelerator of the international thermonuclear experimental reactor," *Phys. Rev. Special Topics Accel. Beams*, vol. 11, no. 1, p. 014202, 2008.

[24] J. R. Dormand and P. J. Prince, "A family of embedded Runge-Kutta formulae," *J. Comput. Appl. Math.*, vol. 6, no. 1, pp. 19–26, 1980.

[25] H. Tawara *et al.*, "Cross sections and related data for electron collisions with hydrogen molecules and molecular ions," *J. Phys. Chem. Ref. Data*, vol. 19, no. 3, pp. 617–636, 1990.

[26] N. Pilan, A. De Lorenzi, and P. Veltri, "Voltage holding prediction in multi electrode-multi voltage systems insulated in vacuum," *IEEE Trans. Dielectr. Electr. Insul.*, vol. 18, no. 2, pp. 553–560, Apr. 2011.

[27] [Online]. Available: http://www.comsol.com

[28] N. Pilan, P. Bettini, A. De Lorenzi, and R. Specogna, "Voltage holding optimization of the MITICA electrostatic accelerator," *Fusion Eng. Des.*, vol. 88, nos. 6–8 pp. 1038–1041, 2013.

[29] F. F. Cap, "Langevin equation of motion for electrons in an inhomogeneous plasma," *Nucl. Fusion*, vol. 12, no. 1, p. 125, 1972.

[30] I. T. Dimov, *Monte Carlo Methods for Applied Scientists*. Singapore: World Scientific, 2008.

[31] R. Ravaud, G. Lemarquand, and V. Lemarquand, "Magnetic field created by tile permanent magnets," *IEEE Trans. Magn.*, vol. 45, no. 7, pp. 2920–2926, Jul. 2009.

[32] R. Latham, *High Voltage Vacuum Insulation*. New York, NY, USA: Academic, 1995.

Authors' photographs and biographies not available at the time of publication.